Available online at www.sciencedirect.com
ScienceDirect
Icarus 191 (2007) 337–351
ICARUS
www.elsevier.com/locate/icarus

Mass–radius curve for extrasolar Earth-like planets and ocean planets

C. Sotin *, O. Grasset, A. Mocquet

Université de Nantes, Nantes Atlantique Universités, CNRS, Laboratoire de Planétologie et Géodynamique, Faculté des Sciences et des Techniques, B.P. 92208, 2 rue de la Houssinière, 44322 Nantes Cedex 3, France

Received 28 July 2006; revised 30 March 2007

Available online 4 May 2007

Abstract

By comparison with the Earth-like planets and the large icy satellites of the Solar System, one can model the internal structure of extrasolar planets. The input parameters are the composition of the star (Fe/Si and Mg/Si), the Mg content of the mantle (Mg# = Mg/[Mg + Fe]), the amount of H_2O and the total mass of the planet. Equation of State (EoS) of the different materials that are likely to be present within such planets have been obtained thanks to recent progress in high-pressure experiments. They are used to compute the planetary radius as a function of the total mass. Based on accretion models and data on planetary differentiation, the internal structure is likely to consist of an iron-rich core, a silicate mantle and an outer silicate crust resulting from magma formation in the mantle. The amount of H_2O and the surface temperature control the possibility for these planets to harbor an ocean. In preparation to the interpretation of the forthcoming data from the CNES led CoRoT (Convection Rotation and Transit) mission and from ground-based observations, this paper investigates the relationship between radius and mass. If H_2O is not an important component (less than 0.1%) of the total mass of the planet, then a relation $(R/R_{\text{Earth}}) = a(M/M_{\text{Earth}})^b$ is calculated with $(a, b) = (1, 0.306)$ and $(a, b) = (1, 0.274)$ for $10^{-2}M_{\text{Earth}} < M < M_{\text{Earth}}$ and $M_{\text{Earth}} < M < 10M_{\text{Earth}}$, respectively. Calculations for a planet that contains 50% H_2O suggest that the radius would be more than 25% larger than that based on the Earth-like model, with $(a, b) = (1.258, 0.302)$ for $10^{-2}M_{\text{Earth}} < M < M_{\text{Earth}}$ and $(a, b) = (1.262, 0.275)$ for $M_{\text{Earth}} < M < 10M_{\text{Earth}}$, respectively. For a surface temperature of 300 K, the thickness of the ocean varies from 150 to 50 km for planets 1 to 10 times the Earth's mass, respectively. Application of this algorithm to bodies of the Solar System provides not only a good fit to most terrestrial planets and large icy satellites, but also insights for discussing future observations of exoplanets.

Keywords: Extrasolar planets; Ices; Exobiology; Equation of state; Terrestrial planets

1. Introduction

The discovery of extra-solar planets opens a new era in planetary science and raises the question of life-sustaining planets in the interstellar space (Stevenson, 1999). The search for Earth-like planets becomes an appealing and technically challenging research topic. So far, most of the extra-solar planets are giant planets close to their star because the detection methods require short orbital periods (close to the star) and large masses and large diameters to mask sufficiently the light from the star (transit method) and/or to affect the motion of the star so that Doppler shifts can be detected. At the time of writing this paper, these two methods have allowed the discovery of more than 200 planets (Schneider, The Extrasolar Planets Encyclopaedia, http://exoplanet.eu/catalog.php). Although observations such as the size of the planet and its distance to the star, are mainly confined to giant planets close to their star, these discoveries have already changed our understanding of planet formation (e.g. Lin et al., 1996; Trilling et al., 1998) and have opened our minds to the diversity of planets.

Recently, Rivera et al. (2005) reported on the discovery of a planet 7.5 times the mass of the Earth. This is an important step toward the discovery of Earth-like planets which are believed to be at most 15 times the mass of the Earth in order not to retain a primordial atmosphere of H_2 and He (Wuchterl et al., 2000). Another important discovery is the detection of OGLE-2005-390-Lb by gravitational lensing around a M star (Beaulieu et al., 2006). This planet would have a mass equal to $5.5^{+5.5}_{-2.7}$ times the Earth's mass. Both planets do not orbit their star in the so-called 'habitable zone': the first planet is too close to its star (0.02 AU) and the second one orbits its star at about

* Corresponding author. Fax: +33 (0) 251 12 5268.
E-mail address: christophe.sotin@univ-nantes.fr (C. Sotin).

0019-1035/$ – see front matter
doi:10.1016/j.icarus.2007.04.006

5 AU, a distance where the black body temperature is about 50 K. But it is likely that the discovery of Earth-like planets in the 'habitable zone' will happen in the near future and one goal of the paper is to provide a relationship between mass M and radius R for Earth-like planets up to 15 times the Earth's mass. In addition, since many planets are expected to form outside the "snow-line," this study also investigates the relation $R(M)$ when water amounts are large and form the so-called ocean-planets (Léger et al., 2004).

The present study was triggered by the preparation of the CNES lead CoRoT (Convection, Rotation and Transit) mission (Rouan et al., 1999; Borde et al., 2003) and has already been reported at various meetings (e.g. Dubois et al., 2002). The physical approach is quite similar to the approach of Valencia et al. (2006). The main difference of the present model is that the composition of the planet is fixed by the composition of the star. This constraint is supported by the observation that meteorites that are representative of the planetesimals that formed the planets, have a chemical composition similar to the Sun (e.g. Däpen, 1999). Since the composition of stars can be obtained in many cases (e.g. Huang et al., 2005), it seems appropriate to use it as the compositional constraint for the orbiting planets. With this approach, it is not necessary to fix the size of the metallic core, a parameter highly uncertain even for bodies of the Solar System. Another major difference with previous papers is the determination of the mass–radius relationship for ocean planets.

The next section describes the model used to obtain the relationship between mass and radius. It includes a description of elementary composition and petrology of the different shells that are supposed to compose this kind of planets. It also includes a comparison with the density profile known for the Earth from inversion of seismic data and a comparison with the radius–mass values known for solar bodies. The results of the model are described in Section 3 for both Earth-like planets and ocean-planets. Finally, we discuss the results and the main uncertainties for their application to exoplanets.

2. Model

This section describes how a set of five independent parameters (Mg/Si, Fe/Si, Mg#, mass fraction of H_2O, total mass) is used to describe the composition of the different layers in the planet (Sections 2.1 and 2.2). Then, the temperature profile within each shell and at its interface is provided according to our present knowledge of heat transfer within the Earth and other Earth-like planets. The iterative process that provides pressure, density and thickness of each shell is then described. For clarity in the text, the equations of state (EoS) that link temperature, pressure and volume for each phase are described in an appendix. Robustness of the model will be presented in the result Section 3.1.

2.1. Main characteristics of the layers

An exoplanet would be composed of five shells (Fig. 1): the core, the lower and upper silicate mantles, the high-pressure ice outer shell and the hydrosphere. The silicate crust is considered as part of the upper-mantle layer since its mass is negligible

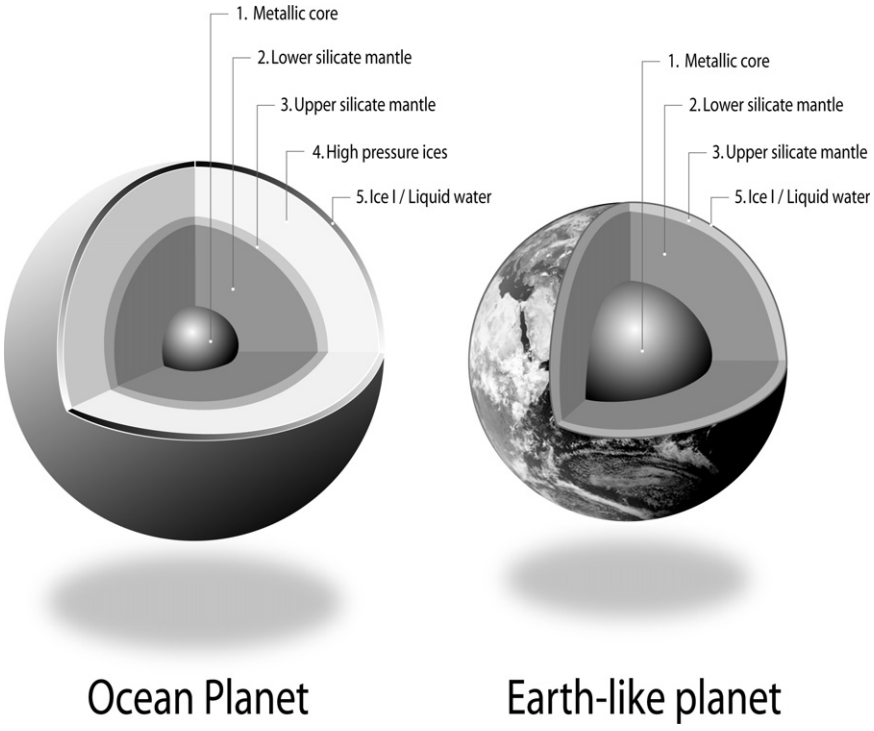

Fig. 1. Interior model of Earth-like and ocean exoplanets. The description of the different layers is detailed in the text. The thicknesses of the layers are not to scale, but their relative sizes between the two planetary families are correct. For a given mass, an ocean exoplanet has a smaller metallic core and silicate mantles and a larger radius than an Earth-like planet. In the case of ocean planets, the upper silicate mantle, composed of olivine and pyroxenes, may not exist if the amount of H_2O is such that the pressure at the ice/silicate interface is larger than that of the olivine to Mg-perovskite + magnesiowüstite transformation.

compared to that of the silicate mantle. For an Earth-like planet, the layer of high pressure ices does not exist since the amount of water is very small. In the case of an ocean planet, it is the upper silicate layer which does not always exist. The pressure at the bottom of the icy shell can be so high that low-pressure minerals of the upper mantle are not present.

- *Layer 1*: The innermost layer is the iron-rich core. It is assumed to be a liquid layer formed in the Fe–FeS system with 87% of pure iron. This choice is driven by the following terrestrial observations. Seismic data suggest that a light element is present. Although we do not have evidence that this light element is sulfur, it is chosen due to its compatibility with liquid iron and to the lack of sulfur in the mantle and in the crust compared to solar abundances (Poirier, 1994). Laboratory experiments (Boehler, 1992; Yoo et al., 1993) suggest that the melting temperature of Fe–FeS alloy is lower than the melting temperature of silicates. Since the mantle temperature has to be close to its melting point in order to transfer heat by subsolidus convection, the mantle temperature is likely to be larger than the melting temperature of the Fe–FeS alloy. This is true for the Earth. According to recently processed data (Yoder et al., 2003) this is also true for Mars, a planet that is only one tenth of the Earth's mass. During the differentiation process that leads to the formation of the core, part of the gravitational energy is turned into heat (e.g. Solomon, 1979). The larger the planet, the more gravitational energy involved in the differentiation and the larger the core temperature. It is therefore expected that the initial core temperature is larger than that of the Earth for planets bigger than the Earth. The efficiency of heat transfer by mantle convection in big planets is difficult to model due to the lack of data on viscosity at very high pressure. It is therefore difficult to conclude on the state of the core. The Earth has a small and solid inner core composed of pure iron, whose mass is less than 2% of the Earth's mass. Assuming that the inner core is liquid and not solid does not provide the density jump observed in the Preliminary Reference Earth Model (PREM) as shown in Fig. 2. However, the error in radius is negligible as will be shown in Section 3.1.
- *Layer 2*: The lower silicate mantle: The mantle is divided into two layers because of the important mineralogical transformation which occurs around 23 GPa. The lower mantle is composed of both perovskite (pv) and magnesiowüstite (mw). Each phase is itself a solid solution of Fe-rich and Mg-rich components (Table 1). This composition is deduced from what we know on Earth. We argue that, due to the very large stability fields of high pressure silicate phases, it is reasonable to assume that the lower mantle of any planet is mainly composed of these two phases. The amount of each phase in the mantle and its composition can be computed precisely as will be shown in Section 2.2.
- *Layer 3*: The upper silicate mantle: On Earth, the upper mantle is mostly composed of olivine, ortho- and clinopyroxenes, and garnet (e.g. Vacher et al., 1998). By neglecting calcium and aluminum, the upper mantle is assumed to be simply made of olivine and ortho-pyroxene enstatite. Garnet being denser than the other silicates, our simplification might imply an overestimate of the planet radii. Concerning terrestrial planets, it will be shown in Section 3.1 that this effect must be small since our estimate for Solar System bodies are very good. In the case of ocean planets, the upper mantle does generally not exist because the critical pressure of 23 GPa, above which olivine transforms into perovskite and magnesiowüstite, is achieved within the icy layer.
- *Layer 4*: The high pressure icy layer: Since the model has been set up for studying planets with variable water amount, one can expect large water mantles above silicates. At some depth, liquid water is no longer stable and it is replaced by its high pressure ice polymorphs. Ice VI may be a good candidate below 2 GPa. But the most stable high-pressure phase is ice VII which exists from 2.2 GPa up to

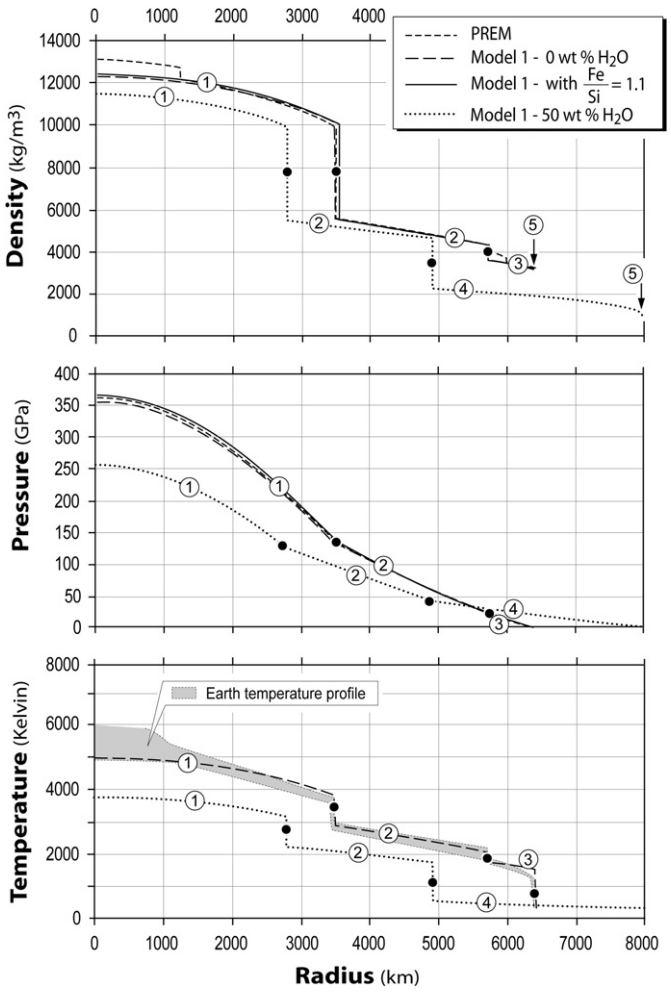

Fig. 2. Density, pressure, and temperature profiles versus radius for an Earth-like planet and an ocean planet. Both planets have a mass equal to $1M_{\oplus}$. Computation is achieved in the simplified (Si, Mg, Fe, S) system using Model 1. For the Earth case, results for density and pressure are compared to PREM (Dziewonski and Anderson, 1981) inferred from seismic data. A comparison of model 1 with its "best fit" counter part (Table 3) is also given. Temperature is plotted in order to provide the valuable range within the Earth but is rather an input parameter than a result (see text for details). Numbers refer to each layer described in Fig. 1. Black dots indicate the location of each interface.

Table 1
List of parameters which describe equation of state parameters, bulk composition of the layers, mineralogical transformations and thermal profiles in the planets

Variable		*Layer 1*		*Layer 2*				*Layer 3*				*Layer 4*		*Layer 5*	
Equation of state/composition															
Equation of state		EoS2		EoS2				EoS1				EoS2		EoS1	
Phases		Iron-rich phase		Perovskite		Magnesiowüstite		Olivine		Enstatite		HP ices		Liquid	
Layer composition (%)		100		x_2		$1-x_2$		x_3		$1-x_3$		100		100	
Components		Fe	FeS	$MgSiO_3$	$FeSiO_3$	MgO	FeO	Mg_2SiO_4	Fe_2SiO_4	$Mg_2Si_2O_6$	$Fe_2Si_2O_6$	Ice VII	Volatiles	Liquid water	Volatiles
Phase composition (%)		87	13	$1-y_2$	y_2	$1-y_2$	y_2	$1-y_3$	y_3	$1-y_3$	y_3	100	0	100	0
Density at ambient conditions (kg/m^3)	ρ_0	8340	4900	4108	5178	3584	5864	3222	4404	3215	4014	1460	–	1000	–
Reference temperature (K)	T_0	300		300		300		300		300		300		300	
Reference Bulk modulus (GPa)	K_0	135		263		157		128		111		23.9		2.2	
Pressure derivative of the bulk modulus	K_0'	6.0		3.9		4.4		4.3		7		4.2		4	
Debye temp. (K)/α parameter (10^{-5} K^{-1})	θ_0/a_T	998		1017		430		2.832		2.86		1470		0	
Gruneisen parameter/α parameter (10^{-8} K^{-2})	γ_0/b_T	1.36		1.96		1.45		0.758		0.72		1.2		0	
Power exponent/α parameter (K)	q/c_T	0.91		2.5		3.0		0		0		1.0*		0	
Nb of atoms/temperature derivative of bulk modulus ($GPa\,K^{-1}$)	n/a_P	–		–		–		−0.016		0		–		0	
References		a, b		c				d, e		f, g		h		i	
Profile															
Upper temp. drop (K)	ΔT	800		300				1200				0		0	
Adiabat (GPa^{-1})	$\gamma_0 - q$	–		–				1.1–1 (arbitrary)				–		Neglected	
References		*j*		*j*				*j*				*k*		*i*	
Phase transition															
Pressure of reference (GPa)	P_0			25								2.216			
Reference temperature (K)	T_0			800								355			
Pressure slope (GPa/K)/ Simon equation coeff.	a	–		−0.0017								0.534			
-/Simon equation coeff.	c			–								5.22			
References		–		*l*								*m*			

These values are based on Earth values. EoS1 and EoS2 refer to the equations of state described in Appendix A. Note that for layer 5 (hydrosphere), only a 2nd order approximation in strain is used. References are: (*a*) Uchida et al. (2001); (*b*) Kavner et al. (2001); (*c*) Hemley et al. (1992); (*d*) Duffy et al. (1995); (*e*) Bouhifd et al. (1996); (*f*) Vacher et al. (1998); (*g*) Anderson et al. (1991); (*h*) Fei et al. (1993); (*i*) Lide (2005); (*j*) Poirier (2000); (*k*) Hobbs (1974); (*l*) Irifune (1987); (*m*) Mishima and Endo (1978).

* Due to the very high uncertainty on q determination for ice VII, the standard value of 1 (within the range of the estimate from Fei et al., 1993), has been preferred because it provides an adiabat which remains stable above 60 GPa.

36 GPa at least (Munro et al., 1982; Hemley et al., 1987). Thus, ice VII has been chosen as the main component of these possible icy mantles. Above 40–50 GPa, it is admitted that ice VII transforms into ice X (Hemley et al., 1987; Schwager et al., 2004). Ice X is stable up to at least 150 GPa. For very massive ocean planets, such a pressure can be achieved in the ice shell. But transition from ice VII to ice X being rather continuous, a single equation of state from low pressure up to 130 GPa is generally proposed (Hemley et al., 1987).

- *Layer 5*: The hydrosphere: Depending on the surface temperature and pressure conditions, water can be either in the liquid state or in the solid state. The physical state of water is of fundamental importance for exobiology, but it does not strongly influence our results. Indeed, despite noticeable discrepancies between ice I and liquid physical parameters (density, thermal expansion coefficient, heat capacity), this upper layer is always very thin compared to the planet size, so that our results do not depend on its solid or liquid state. The liquid state has thus been chosen arbitrarily.

2.2. Bulk composition of the planets

An exact estimate of the composition of icy layers is out of the goal of this paper. It will simply be assumed that they are composed of pure ice. Silicate mantles and the core are composed of mineral phases which combine the following eight elements: Si, Mg, Fe, O, Ca, Al, Ni, and S. Four elements (Si, Mg, Fe, O) provide 95% of the total mass (silicates + core). With the four next more abundant elements (Ca, Al, Ni, S), then 99.9% of the mass is explained. However, these four minor elements add a lot of complexities in the system whereas little error (less than 1% in mass) is made by adding these elements to their closest major element. Ni behaves like Fe, most of the sulfur is present in the iron core, Al is equally divided between Mg and Si in order to account for charge conservation, and Ca is added to Mg. In this first attempt, the minor elements are neglected. The consequences of this assumption are discussed in Section 4.

Following the above assumptions, the independent parameters required to fix the composition of a planet are: (1) the H_2O mass relative to the mass of the planet (M_{H_2O}); (2) the Mg/Si mole fraction; (3) the Fe/Si mole fraction; (4) the Mg# (Mg number) defined as the mole fraction Mg/(Mg + Fe) in the silicates. With these four parameters, both the size of the different layers and the mineralogical composition of the silicate mantles can be deduced if three more assumptions are made on the composition of the layers.

- Water is located in layers 4 and 5. The amount of water incorporated into silicates is neglected considering that this amount is less than 0.1%. This assumption allows us to link directly the position of the interface between silicates and ices using M_{H_2O}.
- The composition of the core is fixed to $Fe_{0.87}$–$FeS_{0.13}$, which is based on what is known for Earth although the nature of the light element in the Earth's core is still debated (e.g. Poirier, 1994).
- The mantle is supposed to be chemically homogeneous so that the limit between the upper mantle and the lower mantle is only understood as the mineralogical transformation of ringwoodite. It means that both Mg# and Mg/Si are constant throughout the mantle.

If y_2 and y_3 are the iron content of each phase in the lower and upper mantle, respectively (Table 1), then:

$$\mathrm{Mg\#} = \left(\frac{\mathrm{Mg}}{\mathrm{Mg}+\mathrm{Fe}}\right)_{\mathrm{silicates}} = 1 - y_2 = 1 - y_3. \tag{1}$$

Magnesium and silicon are only found in the upper and lower mantle so that the ratio Mg/Si for each mantle must equal the input ratio. The lower mantle is composed of perovskite ([Mg,Fe]SiO_3) and magnesiowüstite ([Mg,Fe]O). The upper mantle is modeled with two phases: olivine ($[Mg,Fe]_2SiO_4$) and pyroxene ($[Mg,Fe]_2Si_2O_6$). If x_2 and x_3 are the proportion of perovskite (pv) and olivine (ol) in the lower and upper mantle (Table 1), then:

$$\left(\frac{\mathrm{Mg}}{\mathrm{Si}}\right)_2 = \left(\frac{\mathrm{Mg}}{\mathrm{Si}}\right)_3 \Leftrightarrow x_2 = 1 - x_3/2, \tag{2}$$

with indices referencing the layers. For a given value of x_2, the amount of iron is fixed in the mantle with Eqs. (1)–(2). Iron being present in the silicate mantles and in the core, the ratio Fe/Si links the mass (and the size) of the metallic core (M_1) with x_2. But there is only one set (x_2; M_1) which provides the correct mass for the whole planet. In practice, the model is based on an iterative scheme (see Section 2.4 for details) which computes the unique internal structure consistent with the total mass of the planet, and with the four parameters that constrain the composition of the layers: M_{H_2O}; Fe/Si; Mg/Si; Mg#.

With the assumption that the composition of a planet is fixed by the molar abundances of its host-star, recent values for solar abundances (Däpen, 1999) suggest that Fe/Si and Mg/Si can be fixed to 0.977 and 1.072, respectively (Table 2). The amount of water and the silicate Mg# are free parameters which cannot be constrained easily. Based on what we know in the Solar System, the amount of water can vary from almost 0 for the inner planets (the Earth contains between 2.5 and 5×10^{-4} Earth's mass of water) to roughly 50% of the total mass in the icy satellites of giant planets. The Mg# is largely unknown except for Earth (∼0.9) and Mars (∼0.7) and will be investigated. Its value depends on the degree of differentiation of a planet. The more differentiated the planet is, the larger is the value of Mg#.

Assuming a solar composition for the bulk composition of a planet is still debated. Although CI chondrites have a solar composition, it has been suggested (Javoy, 1995) that the composition of the Earth may be similar to that of EH enstatite chondrites. In this case, rocks are more Si-rich and the ratio Mg/Si and Fe/Si are lowered to 0.734 and 0.878, respectively (Table 2).

These values neglect the presence of Ca, Al, Ni, and S. If these elements are added to the major ones that occupy the same kind of sites as described in the first paragraph of this section,

Table 2
Characteristics of the four models used to test the calculations for Solar System bodies

	Solar[a]	Solar[b]		EH[a]	EH[b]	
		Model 1	Model 2		Model 3	Model 4
M_{H_2O}	–	5×10^{-2}–50	5×10^{-2}–50	–	5×10^{-2}–50	5×10^{-2}–50
(Fe/Si)	0.977	0.986	0.986	0.878	0.909	0.909
(Mg/Si)	1.072	1.131	1.131	0.734	0.803	0.803
Mg# (silicates)	–	0.9	0.7	0.9–0.7	0.9	0.7

The compositions of the silicate mantle and the size of the core are constrained by the Fe/Si, Mg/Si and Mg# parameters. For comparison, both solar and EH enstatite chondrites values are indicated. These two models are end-member models that are described in the text. For each composition, the first column indicates the solar value and the two other columns give values for Mg# equal to 0.9 and 0.7, respectively. In these two columns, the minor elements (Ca, Al, Ni) are replaced by the major elements as described in the text. The amount of water is fixed relatively to the total mass of the planet either to 5×10^{-2} wt% (Earth-like planets) or to 50 wt% (ocean planets).

[a] Values with only Si, Mg and Fe.

[b] Al, Ca and Ni replaced by Si, Mg, Fe (see Section 2.2 for details).

then the ratios Fe/Si and Mg/Si become a little bit larger and equal to 0.986 and 1.131, respectively (Table 2). For the solar composition, the ratios Mg/Si and Fe/Si become 4 and 1% larger, respectively. With the enstatite model, these ratios become 9 and 4% larger. This discussion shows that composition parameters are uncertain, even for the Solar System. Therefore, the two extreme cases (solar abundances/EH enstatite composition) will be tested.

A precise description of the results will be given in Section 3.1 but it can be already noted that varying molar ratios Fe/Si and Mg/Si in the range discussed above causes small differences on computed planetary radii (3‰ in average). It is the amount of water which strongly influences the radius for a given planetary mass. The three other parameters (Fe/Si, Mg/Si, and Mg#) mainly control the size of the core and the amount of iron in the silicate mantle.

2.3. The thermal profile within the planets

Study of the Earth has told us that even in the solid mantle, heat is transferred by subsolidus convection. The temperature of the Earth's mantle is at most a few hundreds of degrees lower than melting temperature (Zerr et al., 1998). In large planets, the temperature in the silicate mantle is controlled by the competition between the heating due to the decay of long-lived radiogenic elements and the cooling by subsolidus convection that is more and more efficient as temperature increases and viscosity decreases (Tozer, 1972).

The thermal profile within the Earth is characterized by adiabatic paths within the convecting layers, and by important temperature variations at the interfaces where thermal boundary layers build up until they become unstable to convection. The temperature difference (ΔT) at each interface of this model has been fixed according to the Earth case (Poirier, 1994; Table 1). Since we assume vigorous convection, the thicknesses of thermal boundary layers are neglected. This simple approximation provides a reasonable estimate of the Earth thermal profile (Fig. 2) and it will be applied throughout the paper. Nonetheless, for very large planets, one must keep in mind that we have little constraint on the temperature difference at each interface although the temperature must not be too far from the melting point for convection to operate.

For both liquid and solid layers, convection is assumed vigorous so that the temperature profile in the convective zone is adiabatic:

$$\frac{\mathrm{d}T}{\mathrm{d}P} = \frac{\alpha T}{\rho C_P} = \frac{\gamma T}{\rho \Phi}, \tag{3}$$

with γ and Φ the Grüneisen and the seismic parameters, respectively:

$$\gamma = \gamma_0 \left(\frac{\rho_0}{\rho}\right)^q, \tag{4}$$

$$\Phi = \frac{K_S}{\rho} = \frac{\mathrm{d}P}{\mathrm{d}\rho}. \tag{5}$$

In Eqs. (3)–(5) T, P, ρ, α and C_p are temperature (K), pressure (Pa), density (kg/m^3), thermal expansion coefficient (K^{-1}) and heat capacity (J/kg/K), respectively. The temperature within each layer can be computed using (3)–(5). Parameters are relatively well constrained (Table 1) at pressure values relevant to the Earth's case, except for the high pressure ice shell. In that case, the surprising negative value of q proposed by Fei et al. (1993) does not allow us to extrapolate the adiabatic profile above 60 GPa. Thus, the common value $q = 1$ has been preferred in this layer. In general, parameters γ_0 and q proposed in Table 1 are only correct for a moderate pressure and temperature range. By applying Eqs. (3)–(5) in much larger pressure domains, we expect important deviations of the computed thermal profiles to the real ones. But at present time, there is no way to provide an accurate model for large planets because no experimental constraints on equation of state are available for very large pressures and temperatures relevant to the deep interior of these bodies (see Figs. 3 and 4).

2.4. Modeling the deep interior

The relation between the mass of a planet and its size is derived from the expression of the total mass, knowing the density distribution:

$$M_p = 4\pi \int_0^{R_6} r^2 \rho(r)\,\mathrm{d}r \tag{6}$$

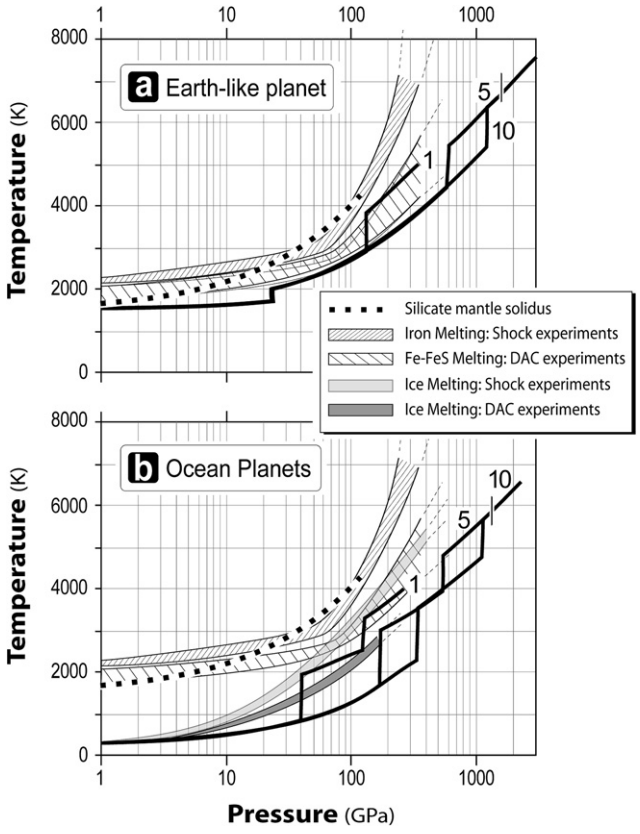

Fig. 3. Comparison between temperature profiles and melting curves of H_2O and iron alloys. Melting domains of iron (Williams et al., 1987; Anderson and Ahrens, 1994, 1996; Boehler, 1993; Alfe et al., 2002) and ice VII (Mishima and Endo, 1978; Fei et al., 1993; Frank et al., 2004) are plotted as a function of pressure. Above these domains, the component is always liquid. A large discrepancy exists between data obtained with static experiments (e.g. Diamond anvil cell (DAC) experiments) and those acquired with dynamic pressure experiments (e.g. shock experiments). This difference is commonly explained by a "superheating" effect during shocks at large pressures (Koenig et al., 2004). Data are highly uncertain above 200 GPa. In the case of iron and for static experiments, the lowest curve is for the melting of FeS while the upper curve corresponds to pure iron. One may expect the melting of a Fe–FeS system anywhere within this domain. (a) Earth-like planets: Thermal profiles for 1, 5 and $10M_\oplus$ are above the melting curve of the FeS component in the core (P, T) domain. (b) Ocean-planets: the transition from liquid to ice VII occurs at low pressure (between 1 and 2 GPa depending on the surface temperature). The ocean, if it exists, cannot be represented. The iron core is probably liquid, but whatever the planetary mass, it is colder and at lower pressure than for the Earth-like case.

with R_6 the radius of the planet. The main problem consists in providing a good estimate of the density profile within the planet. Since each layer has its own composition, the integral of Eq. (6) is split in five parts to allow the computation of the density using the equation of state (EoS) of the main constituents of the layer:

$$M_p = 4\pi \sum_{i=1}^{5} \int_{R_i}^{R_{i+1}} r^2 \rho_i(r)\,\mathrm{d}r \tag{7}$$

with i the reference number of each layer and $R_1 = 0$. The density within each layer is computed using appropriate thermal EoS. Depending on the experimental constraints available and on the temperature field, a third-order Birch–Murnaghan is used with a thermal correction incorporated either in the thermal expansion (Eq. (A.1)) or using a Debye formulation with a thermal pressure term (Eq. (A.2)). Details of calculation and argumentation about the choice of EOS for each layer can be found in Appendix A. The parameters required for each EOS are given in Table 1.

Density depends strongly on pressure and temperature. Temperature is computed as described in Section 2.3 while pressure is computed in each layer using:

$$P_i(r) = P(R_{i+1}) + \int_{r}^{R_{i+1}} \rho_i(x) g_i(x)\,\mathrm{d}x \tag{8}$$

with

$$g_i(r) = g(R_i)\left(\frac{R_i}{r}\right)^2 + \frac{4\pi G}{r^2} \int_{R_i}^{r} x^2 \rho_i(x)\,\mathrm{d}x \tag{9}$$

with $i \in [1, 5]$ and $r \in [R_i, R_{i+1}]$. Equations (7)–(9) cannot be used if an estimate of the interface radii is not provided. In the following section, a brief description of the iterative scheme used in the model for computing the position of the interfaces knowing the composition of the planet (Section 2.2) is provided.

The model starts from an initial internal structure which is defined using constant density within each layers. Furthermore, the core mass fraction is fixed to an initial value. The interfaces are defined arbitrarily and the temperature is computed using the adiabatic profiles described in Section 2.3. Computation of gravity and pressure profiles within the planet is achieved with Eqs. (8)–(9). The density profile is then obtained using the EOS relative to each layer. It is then possible to compute a new estimate of the planetary interfaces.

First, the radius of the core (R_2) is computed using the fixed core mass fraction and the density profile in the core. The radius of the lower—upper silicate mantle interface (R_3) is easily found because it corresponds to the mineralogical transformation of the high pressure phase of olivine (i.e. ringwoodite) to Mg-perovskite and magnesiowüstite. This transformation has been extensively studied both theoretically and experimentally due to its fundamental importance for understanding the Earth mantle dynamics and structure (Ita and Stixrude, 1992). It varies linearly with temperature from 25 GPa (800 K) down to 23 GPa (2000 K). Thus, the interface is computed in the model using the simple equation $P = P_0 + a \times (T - T_0)$ with parameters described in Table 1. Basically, the upper mantle does not exist above roughly 24 GPa. In practice, this means that in the cases where the amount of water is important, the pressure in the silicates in contact with ice VII will be high enough for impeding the existence of the olivine/enstatite layer. The silicate mass fraction being equal to $M_\mathrm{p} - M_{\mathrm{H_2O}} - M_\mathrm{core}$, it is then possible to compute the radius R_4 (silicate–ice interface) which respects the total mass of silicates in the planet. Finally, the transition from liquid to ice (radius R_5) is well described using a Simon equation:

$$P = P_0 + a\left((T/T_0)^c - 1\right). \tag{10}$$

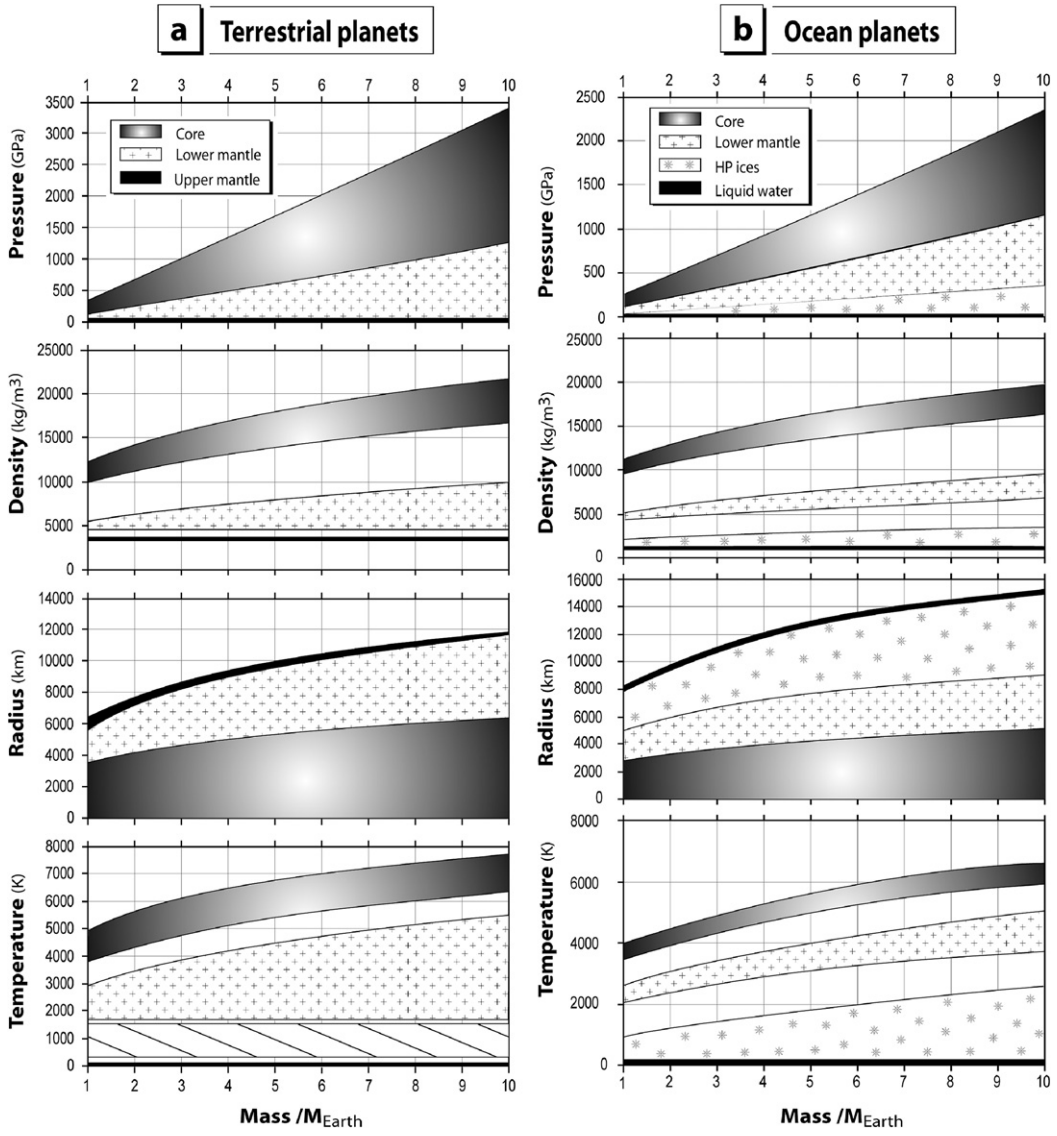

Fig. 4. Internal structure of terrestrial and ocean exoplanets as a function of mass (Model 1). For each layer, pressure, density, size and temperature variations through the layer are plotted. The surface liquid layer being always thinner than 1 km is not shown. Boundaries of each domain indicate the characteristics on the interfaces. From 1 to $10M_{\oplus}$, both pressure at the base of the mantle and in the center are multiplied by almost 10, while the average density within the core and the lower mantle is only 1.7 times higher. The planetary radius is roughly multiplied by two from 1 to $10M_{\oplus}$. One can note the importance of the high pressure icy mantle that is more than 6000 km thick for a $10M_{\oplus}$ planet!

An accurate fit has been provided by Mishima and Endo (1978) up to 15 GPa and by Fei et al. (1993) up to 20 GPa but using a more sophisticated equation. This interface is placed in the model depending on the P–T profiles within the water-rich layer. Parameters describing the Simon equation are shown in Table 1. Note that if the amount of water is very small, the ice VII layer does not exist (terrestrial planets, Europa) and silicates are directly in contact with the liquid layer ($R_4 = R_5$). The radius of the planet R_6 is then computed in order to have a total mass of water equal to M_{H_2O}.

At the end of this procedure, the computed internal structure respects four of the five input parameters: Mg# and Mg/Si (see Section 2.2), M_p, and M_{H_2O}. The ratio Fe/Si is then computed and compared to the input value. A new core mass fraction is estimated using the bisection method and the model iterates the computation of temperature, density and pressure profiles. It stops once the computed Fe/Si is almost equal to the Fe/Si input (difference lower than 5‰).

3. Results

3.1. Calculations for Solar System bodies

The algorithm described in the previous section has been tested for solid objects of the Solar System whose internal structure is constrained by observations. For all these objects, the reference elementary composition (Mg/Si and Fe/Si) is the solar composition (Table 2). As described below, we have also used the EH composition proposed by Javoy (1995, 1999), which represents another end-member. The Mg# has also been varied. The difference between these extreme models is less than 1% in radius (Table 3), which is quite negligible. Therefore, in the

Table 3
Comparison of the radius observed for the Solar System bodies and the predictions given by our modeling

Name	Mass/M_{Earth}	Planetary radius					Best fit			
		Measured	Model 1	Model 2	Model 3	Model 4	Model 1	Model 2	Model 3	Model 4
Water-rich							M_{H_2O} (%)			
Europa	*0.008*	*1565*	1854	1865	1852	1860	15	13	16	14
Callisto	0.0181	2410	2396	2407	2397	2403	51	49	50	50
Ganymede	0.0248	2631	2641	2655	2638	2650	50	47	49	48
Titan	0.0225	2575	2563	2577	2559	2575	51	49	51	50
Earth-like							Fe/Si			
Mercury	*0.055*	*2437*	2705	2723	2706	2715	8	8	7.5	7.5
Mars	0.107	3389	3349	3366	3342	3357	0.78	0.84	0.71	0.79
Venus	0.81	6051	6056	6071	6008	6032	0.96	1.03	0.80	0.85
Earth	1	6371	6414	6447	6379	6405	1.10	1.19	0.92	0.99
Moon	*0.0123*	*1738*	1600	1642	1591	1621	0.22	0.48	0.30	0.30

The right part of the table indicates the required value of M_{H_2O} (ocean-planet) or Fe/Si (Earth-like planet) in order to get the value of the measured radius for each body and for each of the four models described in Table 2.

rest of the study, the solar composition will be the reference for the models.

For Earth, the information on the radius of interfaces, the pressure profile and the density profile come from seismic data that have been acquired since the beginning of the 20th century. The location of the interfaces are well constrained but the composition of the deep layers relies on the assumption that the bulk composition is chondritic. In the results described in Fig. 2, the Fe/Si, Mg/Si and Mg# are those of Model 1 given in Table 2. The fit is quite good for the pressure and density, which are two data provided by seismic inversion (Dziewonski and Anderson, 1981). The value of the radius is 43 km (0.7%) larger than the value of 6371 km. Considering the assumptions made for this simulation, and in particular the fact that only four elements are taken into account (Si, Mg, Fe, O), the fit is considered as quite good. The temperature profile predicted for the Earth is obviously close to the expected one since information from Earth were used to calculate the temperature profile. It is interesting to note that the value of Fe/Si that would provide an exact fit to the radius is 1.10 (Fig. 2; Table 3), a value that is only 2.5% lower than the solar value.

The same model has been applied to Mars and Venus. For Venus, the Earth-like model (Mg# = 0.9) gives a radius only 5 km (0.1%) larger than the observed value. It suggests that the Earth-like model applies very well to Venus, an observation that was already made by Anderson (1980). For Mars, taking a terrestrial value for the Mg# gives a radius that is 40 km (1.5%) smaller than the measured value (Table 3). However, the measurements made on SNC meteorites suggest that the Mg# for Mars is smaller than the Earth's value (Dreibus and Wänke, 1985). If one takes Mg# = 0.7 then the radius is only 23 km (0.7%) smaller (Table 3). A smaller value of the Mg# means that less iron differentiated into an iron core, which is in agreement with recent estimates of the core radius (Yoder et al., 2003). Values of Mg# on the order of 0.75 have been calculated in order to explain the chemical composition of the basaltic meteorites supposed to come from Mars (Dreibus and Wänke, 1985).

For Mercury and the Moon, two objects that are much smaller than the Earth, the fit is not as good because these two bodies had very different accretions. Applying the Earth's model gives a radius 12% larger for Mercury and 8% smaller for the Moon. There are three scenarios that have been proposed to explain Mercury's large density (Cameron et al., 1988): the equilibrium condensation scenario, planetary evaporation of the crust and part of the mantle, and a major planetary collision. The first and third scenarios seem unlikely (Cameron et al., 1988). On the other hand, the vaporization scenario (Fegley and Cameron, 1987) predicts elementary composition of the surface that will be tested by two forthcoming missions: the NASA Messenger mission and the ESA Bepi Colombo mission. It is interesting to note that the size Mercury would have if it had the same ratio than the other terrestrial planets is 640 km less than Mars. It suggests that even without vaporization, the planet closest to the star would have been quite small. The fact that Mercury, the planet closest to the Sun, has a much larger Fe/Si ratio than the solar one must be noted in order to be careful when interpreting the observations (mass and radius) of exoplanets close to their star (see discussion). For the Moon, the situation is also different because the Moon formed as the Earth had already differentiated into an iron-rich core and a silicate mantle. Therefore the Fe/Si ratio for the Moon is much less than the solar value. A value of 0.22 for the Fe/Si ratio is found in order to find the exact value of the radius (Table 3). In this case, the Moon would have an iron core 405 km in radius. Such a value is in agreement with values proposed by Kuskov and Kronrod (2001).

This model has also been applied to determine the radius of the large icy satellites of the Solar System. Although these bodies are much too small to be detected in other Solar Systems, they provide some insight on what could be ocean planets. Except for Europa that has much less H_2O than the other large icy satellites, an H_2O mass fraction close to 50% is found for Ganymede, Callisto and Titan (Sotin and Tobie, 2004) if a three-layer structure is assumed (silicate mantle and a layer with the density of ice VI covered by a layer with the density of ice I). This value has been used to model the mass–radius relationship for ocean-planets. The radii of the large icy moons are determined at less than 1% (Fig. 5), which is a very good fit.

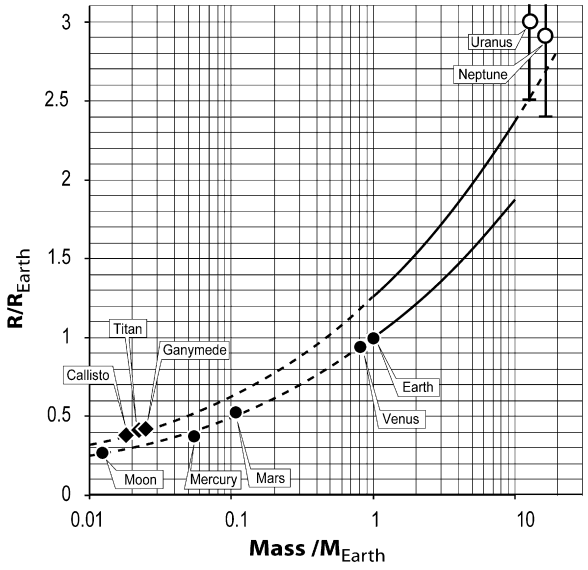

Fig. 5. Mass–radius relationship for Earth-like exoplanets and ocean planets with 50 wt% of H_2O. Radii are divided by the theoretical estimate of the Earth radius in order to get a coefficient equal to 1 before the power exponent in the telluric case. Results are plotted for Model 1 but do not change significantly if an enstatite composition is preferred or if the Mg# is modified within the range [0.7–1.0]. The surprising results is the similar trend for Earth-like and Ocean planets. Two different trends have been obtained for planets less massive than Earth and for planets more massive than Earth. The power exponent varies from 0.306 to 0.274 for low-mass and high-mass planets, respectively. The exponent does not seem to depend on the amount of water. Whatever the mass of the planet, a 50 wt% H_2O planet is predicted to be 25% larger than the terrestrial one.

Finally, the model has been applied to Uranus and Neptune. Although these outer planets have a thick hydrogen-rich outer layer that is not modeled in the present study, they provide points at large masses. It is worth noting the recent discovery of three Neptune-like planets around HD 69830 (Lovis et al., 2006). In order to account for this outer hydrogen rich layer, the radius and the mass of each planet have been reduced by one Earth radius and two Earth masses, respectively (Hubbard et al., 1995; Podolak et al., 2000). Their radius is still larger than the predicted radius with 50% ice (Fig. 5). It is larger by 0.5 and 0.2 Earth radius for Uranus and Neptune, respectively. This can be due to either a larger mass fraction of ice or (and) a thicker hydrogen-rich outer layer (see discussion in Section 4). Hubbard et al. (1995) propose that the mass ratio ice/rock could be as large as 3.55 for Neptune. With this value, the radius predicted by the present model would be 36% larger than that of a terrestrial (ice free) planet. This would predict a radius for Neptune that would be equal to about 2.9 Earth radius, which is the predicted radius once the outer hydrogen-rich layer is removed (Fig. 5). For Uranus, the value is still too low, which suggests that either the outer layer is thicker or that the mass ratio ice/silicates is even larger.

The algorithm described above gives very good results for determining the radius of terrestrial planets and large icy satellites of the Solar System. The differences found for Mercury, the Moon and Europa provide insights for discussing the results that will be obtained by forthcoming observations of exoplanets less than 15 times more massive than the Earth. This algorithm is now applied to terrestrial and ocean exoplanets.

3.2. Terrestrial exoplanets

This study investigates planets up to 15 times the Earth's mass which is roughly the mass of Uranus and Neptune, two planets that have maintained a primitive atmosphere of He and H_2. This paper is the first of a series where we will investigate a variety of stellar composition. In the present work, we limit ourselves to solar abundances for the different elements that formed these exoplanets (Model 1 in Table 2).

The density, the radii of the interfaces, and the temperature range within each shell is displayed in Fig. 4 as a function of planetary mass. It must be noted that there is a lack of experimental data to constrain the EoS of iron and silicates at pressures above 500 GPa (e.g. Poirier, 2000). Such pressures exist within planets that are only a few Earth masses. Therefore more reliable results have to await for laboratory experiments that will confirm ab initio calculations (Volcadlo et al., 1997; Alfe et al., 2002). This point is illustrated in Fig. 3 where the temperature profile is reported versus pressure for planets 1, 5 and 10 times more massive than Earth. It can be noted that the internal pressure is far above the experimental constraints for 5 and 10 Earth masses. The melting temperature of iron alloys is reported in Fig. 3 in order to assess the state of the iron core (Williams et al., 1987; Anderson and Ahrens, 1994, 1996; Boehler, 1993; Alfe et al., 2002). The lower curve for the melting of Fe–FeS alloys suggests that cores would be liquid. However, the large uncertainties on the composition of metallic cores (e.g. Poirier, 1994) and the lack of experimental data beyond 300 GPa make any conclusion very tentative. The state of the iron core is a critical parameter in order to assess the existence of an internal magnetic field that would protect the atmosphere from bombardment of energetic stellar ions that would efficiently erode it. The pressure at the core-mantle interface varies from 135 GPa to more than 1000 GPa for 1 and 10 Earth mass planets, respectively (Fig. 4). The core radius varies from 4000 to 6000 km for these two cases (Fig. 4).

One major goal of this study is to provide a relationship between mass and radius for interpreting the data that will be obtained by future observations. With the assumption that the composition is solar, the following relationship (Fig. 5) is found:

$$R/R_{\mathrm{Earth}} = (M/M_{\mathrm{Earth}})^{0.274} \quad \text{for } M_{\mathrm{Earth}} < M < 10M_{\mathrm{Earth}}. \tag{11}$$

The exponent coefficient is much less than the value 1/3 it would have if the density did not depend on pressure and temperature. Therefore, the mean density of a planet increases as $M^{0.178}$ and the density of a planet 10 times the Earth's mass is about 50% larger than the Earth's mean density (Fig. 6). Discarding the unknown centrifugal acceleration, the surface gravity increases much more rapidly with increasing mass than the prediction made assuming a coefficient equal to 1/3. Surface gravity increases as $M^{0.452}$ whereas it is $M^{1/3}$ for constant density (Fig. 6). A planet 10 times the Earth's mass would

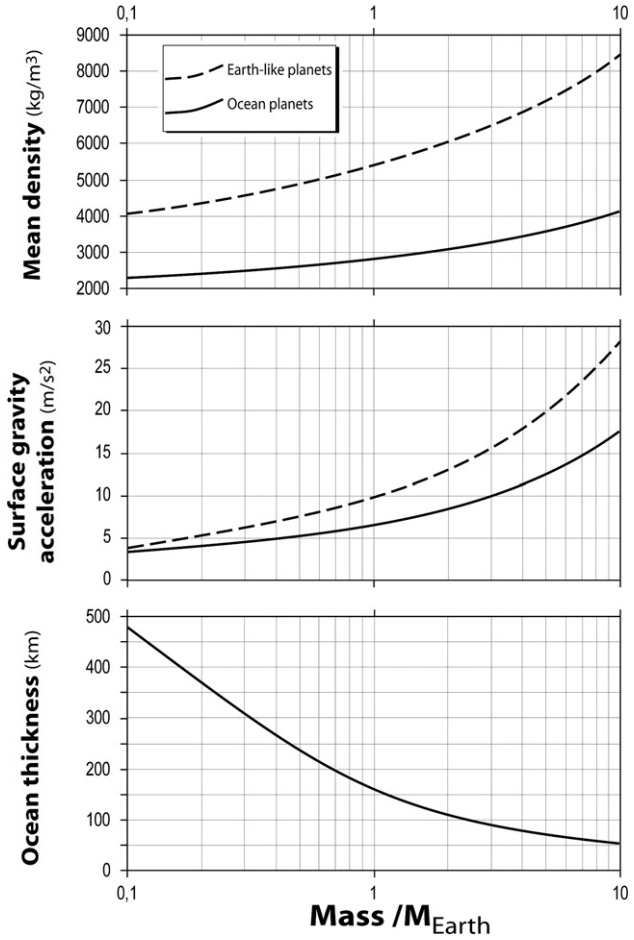

Fig. 6. Mean density (top), surface gravity acceleration (middle), and ocean thickness (bottom) versus mass. The ocean thickness is calculated assuming an isothermal temperature gradient in the ocean. The thickness is controlled by the pressure-dependence of the ice VI melting temperature (see text for details).

have a surface gravity about 3 times that of the Earth. A planet 5 times the Earth's mass would have a surface gravity about twice the Earth's gravity. Accordingly, the radius increases less than the prediction made with constant density: a planet 10 times the Earth's mass would have a radius 2 times larger than that of the Earth.

It must be noted that a relation similar to relation (11) exists for planets smaller than Earth but the coefficient is closer to 1/3:

$$R/R_{\text{Earth}} = (M/M_{\text{Earth}})^{0.306} \quad \text{for } 10^{-2} M_{\text{Earth}} < M < M_{\text{Earth}}. \tag{12}$$

This relation gives a good prediction for solar terrestrial planets (Fig. 5) as it has been already discussed. The cut-off at the Earth's mass is not a particular point. The exponent of the $R(M)$ relationship increases as the mass decreases. We have used this particular cut-off in order to compare our results with those of Valencia et al. (2006).

3.3. Ocean planets

The presence of ocean planets around other stars has been recently proposed (Léger et al., 2004). These planets would have formed in the outer stellar system at a distance where H_2O ice can condense and would have then migrated by a type 2 migration toward their star. The recent discovery of OGLE-2005-BLG-390Lb (Beaulieu et al., 2006) has made this kind of planet quite likely to be detected by forthcoming missions. In order to illustrate the effect of large amount of H_2O, ocean planets having 50% mass H_2O have been investigated in the present study.

Table 4
Coefficients a and b f the law $(R/R_{\text{Earth}}) = a(M/M_{\text{Earth}})^b$ for the different cases explained in the text

M/M_{Earth}	Telluric (0.05 wt%)		Ocean planets (50 wt%)	
	a	b	a	b
0.01–1	1.000	0.306	1.258	0.302
1–10	1.000	0.274	1.262	0.275

The first very intuitive result is that the radius is larger than for terrestrial exoplanets (Figs. 2, 4b, and 5). The radius of an ocean planet having the mass of the Earth is 8000 km, compared to 6400 km for the Earth. The radius of an ocean planet 10 times the Earth's mass is larger than 15,000 km compare to 12,000 km for a terrestrial planet. It is interesting to note that the slope of the mass-radius relationship is almost identical. Therefore, the radius of an ocean planet is 26% larger than that of a terrestrial exoplanet having the same mass (Fig. 5, Table 4). The surface gravity is therefore smaller (63%) than that of a terrestrial planet. Another observation is that pressure, temperature and density in the core are smaller than that of terrestrial exoplanets (Figs. 2 and 4). For a planet 5 times the Earth's mass, the maximum pressure is 1200 and 1700 GPa for ocean planets and terrestrial planets, respectively. Nevertheless, this pressure is larger than the pressures that can be obtained in laboratory experiments. The thickness of the H_2O layer varies from 3000 km for a $1M_{\text{Earth}}$ ocean planet to 6000 km for a $10M_{\text{Earth}}$ exoplanet.

One question that is often asked when considering ocean planets is how deep is the ocean. It is out of the goal of the present paper to investigate the effect of different parameters that affect the thickness of the ocean (heat flow, surface temperature, solutal convection, latitudinal circulation, super rotation). As stated before, the H_2O phase (liquid or solid) does not affect the mass-radius curve. However, some general remarks can be made from this study. Because the temperature gradient in the liquid layer (adiabatic or isothermal or negative like on Earth) is lower than the pressure-dependence of the melting temperature of high pressure phases of ice, the thickness of the ocean is controlled by the intercept of these two temperature profiles. One first important consequence is that the liquid is not in contact with the silicate shell. It means that if volcanism exists in the silicate shell, this volcanism will be in contact with high pressure ice and not with liquid, which gives conditions quite different from those existing on the Earth's seafloor. For sake of simplicity, isothermal gradient is assumed in order to assess how the thickness of the ocean varies with the mass of an ocean exoplanet. Assuming constant temperature, the thickness is controlled by the surface temperature and the gravity acceleration. The non-intuitive result is that the thickness decreases

as the mass increases (Fig. 6). With a surface temperature of 300 K, the liquid layer is 150 km thick for a planet the mass of the Earth and 50 km for a planet 10 times the Earth's mass although the icy layer is 6000 km thick.

4. Discussion

4.1. Comparison with previous models

A previous study on the internal structure of terrestrial exoplanets (Valencia et al., 2006) proposes a law $R/R_{\text{Earth}} = (M/M_{\text{Earth}})^{0.267-0.272}$. The coefficient is the same than the one determined in the present study. The parameters used in the sets of equations (see Appendix A) come from the same sources (Stixrude and Lithgow-Bertelloni, 2005). Although the values for the lower mantle are not given in Valencia et al. (2006), we assume that they are similar to those used in the present study. Both studies use adiabatic gradients in the convective domains. In the present study, the temperature difference at the core–mantle boundary (CMB) is assumed to be equal to 800 K. Such a value is based on the temperature difference in the core and the mantle proposed by Poirier (2000). It is possible that this temperature variation is too large. But as discussed below, the variations due to temperature are small compare to our ignorance of material properties at very high pressure. It is also interesting to note that the models described in Valencia et al. (2006) have a solid iron core whereas the present study assumes a liquid core. Our assumption is based on the hypothesis that the melting temperature of iron alloys is smaller than that of silicates in a pressure range where experimental data are lacking. Whatever is the state of the iron core, the similarity between the two studies suggests that this does not affect much the global relationship between mass and radius. It will be difficult to assess the state of the core by just measuring the mass and radius of an exoplanet.

Another difference with the model of Valencia et al. (2006) is that the present model predicts the modal composition of the silicate layers and uses this composition to compute the EoS parameters. Taking the solar composition (Table 2), the upper mantle is composed of 42% olivine and 58% pyroxene with a Mg# = 0.9. With the same numbers, the lower mantle is composed of 79% perovskite and 21% magnesiowüstite. These numbers are closer to the piclogite model than the pyrolite model that is used to describe mantle composition (e.g. Vacher et al., 1998). But, the modal composition is very sensitive to the (Mg/Si) ratio and a variation of 6% of the ratio gives 32% olivine in the upper mantle. Such variations do not change much the $R(M)$ relationship and will be investigated in further studies.

4.2. Uncertainties on the model

Uncertainties come from the assumptions made to build the model and from uncertainties on the parameters used in the model. The partitioning of iron between the core and the mantle is a major unknown. This is based on the differentiation processes that took place during the formation of the planets. The two end-member models would be a first model with no core (all iron in the mantle phases) and the opposite model with all iron in the core. These models are not realistic considering the internal structure of Solar System planets and were not used as end members in the present study. For a planet the mass of the Earth, the radius would be equal to 6400 km if there is no iron in the mantle and 6478 km if there is no core. For a 5 Earth mass planet, these numbers become 9950 km and 10,030 km, respectively. The difference is only 1%, which is small compared to the 26% difference between a terrestrial and an ocean planet. The presence of an iron core can be established if moment of inertia and/or magnetic field can be measured. Since this may be difficult for extrasolar planets, the measurement of the radius can provide a first hint on the existence of a core. It is important to recall that present models of planetary formation predict the existence of an iron-rich core and that the study of the Solar System suggests that the larger the planet, the larger the iron-core and the smaller the Mg#.

Another simplifying hypothesis of the present study is the way elements such as Al, S, Ni and Ca are taken into account. The amount of each element is added to the amount of Mg, Si and Fe according to their presence in the different phases. This allows us to account for 99.9% of the total mass but phases like the garnet phase is ignored. Garnet is denser than any other phase. It is found only in the upper mantle in amount less than 10%. Considering that this element is about 20% denser than the other phases and that the upper mantle represents only 10% of the total mass of a planet, the error associated to this phase is less than 0.2%, which is quite negligible considering the other hypothesis. Similarly, the crust can be ignored since on Earth, the crust represents less than 2×10^{-5} the total mass. If Si is the light element incorporated into the core, then the radius of the planet is lowered by 1% (less perovskite in the mantle) and the core radius is increased by about 5%.

A major uncertainty related to this kind of model is the lack of experimental constraints on the EoS at very high pressure. Studies on iron have already demonstrated that electronic pressure becomes as large as 10% of total pressure at values larger than 400 GPa (Stixrude et al., 1997). This component is not taken into account in the present calculations. This may lower the exponent of the $R(M)$ relationship. However, it should not change much the difference between ocean planets and terrestrial planets. Forthcoming studies will address this issue based on theoretical estimates of electronic pressure on the calculation of the density of the different materials at pressures larger than 500 GPa (Thompson, 1990).

The temperature profile is another parameter that is largely unknown for planets much larger than the Earth. Although our lack of information could lead to several hundreds of degrees uncertainty on the temperature profile, the resulting variation on the $R(M)$ relationship is small. For example, an error of 100 K on the temperature profile leads to an uncertainty of 0.3% on the volume for a thermal expansion of 3×10^{-5} K^{-1}. The error on the radius is therefore equal to 0.1%. This uncertainty is quite small. Even a temperature error of 1000 K would give only 1% error on the radius. As an example, a test run has been performed for a $5M_{\text{Earth}}$ exoplanet with a temperature 1000 K

larger than the nominal profile described in Fig. 3. The radius becomes equal to 10,074 km instead of 9984 km, i.e. a variation a little bit less than 1%. This variation is once again much smaller than variations between terrestrial exoplanets and ocean exoplanets.

4.3. Additional remarks

The coefficients of the $M(R)$ relationship depend on the formation scenario. For ocean exoplanets that form beyond the snow line and then migrated toward their star, vaporization of the ocean would lower the amount of water and the value of the pre-exponential constant. Ongoing studies are being pursued to determine this coefficient as a function of the total amount of water that could be present in these ocean planets. Similarly, terrestrial planets that formed close to their star may have undergone vaporization processes such as those invoked to explain the depletion of Si on Mercury. In that case, both the preexponential factor and the exponent would be different. Such planets would correspond to the so-called super-Mercury studied by Valencia et al. (2006).

The effect of an outer hydrogen rich layer can be addressed at the light of the results obtained for Uranus and Neptune. As expected, even with a small amount of hydrogen and helium, such planets have a much larger radius than that predicted for terrestrial planets. Since spectroscopic information will be available, the presence of Neptune-like planets will provide additional information on the diversity of planets that can form around stars. It is also interesting to address the evolution of such planets if they move closer to their parent star and loose their hydrogen during this migration. But such studies are out of the goal of the present paper and will be addressed in forthcoming work.

Finally, it is important to discuss the kind of planets that the CNES-led CoRoT mission will be able to detect. This mission was launched on Wednesday 27 December, 2006. A systematic study is being realized using the results of the present work. The possibility to detect an extrasolar planet depends on the distance of the planet to its star and on the diameter of the planet. Preliminary results suggest that a planet orbiting at 1 AU from its star could be detected if its diameter is larger than 25,000 km (=2 Earth radii). Such a planet could be either a big terrestrial planet more than 10 times the Earth's mass or an ocean planet about 5 times the Earth's mass (Figs. 4 and 5).

5. Conclusion

Modeling of the internal structure of Earth-like planets and ocean-planets give relationships between the radius (R) and the mass (M) of a planet. It is assumed that planets have elementary composition similar to that of the star they are orbiting. This assumption has been shown to provide good results for the Solar System bodies. Applied to extrasolar planets more massive than Earth, the radius varies as $M^{0.274}$. This approach allows us to show that ocean planets with 50% H_2O, a value similar to that of large icy satellites, should have radius 26% larger than terrestrial exoplanets. Mid-future space missions searching for planetary transits in the Habitable Zone coupled with Radial Velocity follow-up should provide us with valuable information about their existence and properties. If there are as resistant with respect to evaporation and photolysis of their atmospheres as some models predict, the CNES lead CoRoT mission, which was launched at the end of 2006, should detect the hottest ones.

Acknowledgments

This work was supported by INSU/CNES through its Programme National de Planétologie. We thank Alain Léger and the CoRoT science team for stimulating discussions during their workshops. The careful reviews of Diana Valencia and an anonymous reviewer allowed us to significantly improve the first version of the manuscript.

Appendix A. The equations of state used in the model

Two different approaches are commonly used in Earth sciences for describing both pressure and temperature dependences of materials (for a review see, e.g. Jackson, 1998). Either the effect of temperature is introduced in the parameters which describe the isothermal equation of state of a given mineral, or the thermal effect is taken into account by adding a thermal pressure term to the static pressure obtained from the isothermal equation of state. The first approach is commonly achieved using the 3rd order Birch–Murnaghan equation of state with the thermal effect incorporated into the thermal expansion coefficient:

$$\begin{cases} P(\rho,T) = \dfrac{3}{2}K^0_{T,0}\left[\left(\dfrac{\rho}{\rho_{T,0}}\right)^{7/3} - \left(\dfrac{\rho}{\rho_{T,0}}\right)^{5/3}\right] \\ \qquad\qquad \times\left\{1 - \dfrac{3}{4}(4-K'_{T,0})\left[\left(\dfrac{\rho}{\rho_{T,0}}\right)^{2/3} - 1\right]\right\}, \\ K^0_{T,0} = K_0 + a_P(T-T_0), \\ K'_{T,0} = K'_0, \\ \rho_{T,0} = \rho_0 \exp\left(\displaystyle\int_{300}^{T} \alpha_{T,0}\,\mathrm{d}T\right), \\ \alpha_{T,0} = a_T + b_T T - c_T T^{-2}. \end{cases} \tag{A.1}$$

The relation between pressure, temperature, and density is then described using the eight parameters known at ambient pressure, T_0, ρ_0, K_0, K'_0, a_P, a_T, b_T, and c_T, the reference temperature, density, bulk modulus, pressure and temperature derivatives of bulk modulus, and thermal expansion coefficients respectively. This set of equation provides EoS1.

The second approach dissociates static pressure and thermal pressure that uses the Mie–Grüneisen–Debye formulation:

$$
\begin{cases}
P(\rho,T) = P(\rho,T_0) + \Delta P_{\text{th}}, \\
P(\rho,T_0) = \dfrac{3}{2}K_0\left[\left(\dfrac{\rho}{\rho_0}\right)^{7/3} - \left(\dfrac{\rho}{\rho_0}\right)^{5/3}\right] \\
\qquad\qquad \times \left\{1 - \dfrac{3}{4}(4-K_0')\left[\left(\dfrac{\rho}{\rho_0}\right)^{2/3} - 1\right]\right\}, \\
\Delta P_{\text{th}} = \left(\dfrac{\gamma}{V}\right)\left[E(T,\theta_D) - E(T_0,\theta_D)\right], \\
E = 9nRT\left(\dfrac{T}{\theta_D}\right)^3 \displaystyle\int_0^{\theta_D/T} t^3\,\mathrm{d}t/\left(e^t - 1\right), \\
\theta_D = \theta_{D0}\left(\dfrac{\rho}{\rho_0}\right)^{\gamma}, \\
\gamma = \gamma_0\left(\dfrac{\rho}{\rho_0}\right)^{-q}.
\end{cases}
\tag{A.2}
$$

In that case, the eight required parameters are: T_0, ρ_0, K_0, K_0', θ_{D0}, n, γ_0, q, reference temperature, density, bulk modulus, pressure derivative of bulk modulus, reference Debye temperature, number of atoms per chemical formula, reference Grüneisen parameter, and power exponent, respectively. This set of equation provides the second choice for the equation of state (EoS2).

Choosing between equations EoS1 and EoS2 for describing the P–ρ–T relations within a planetary layer is not straightforward. Many researchers provide both parameters sets for fitting their experimental results. For the upper mantle, EoS1 is the most common EoS, while EoS2 is preferred for describing the core behavior. Concerning Earth's studies, both EoSs are indifferently used for the lower mantle.

In this study, we are dealing with planets more massive than Earth. The thermal pressure term might be quite important which requires a precise description. EoS1 is good as long as the temperature remains within the variations encountered in the Earth mantle because the thermal dependence of the thermal expansion coefficient α has only been fitted in this relevant range. Simple tests above the Earth adiabat indicate that EoS1 overestimates the thermal pressure term while EoS2 provides estimates close to other equations of state derived from ab initio calculations and shock experiments (Thompson, 1990). In addition, high pressures in these massive planets would require the development of the deformation up to the fourth order. However, we lack experimental data on the second derivatives of the bulk modulus, which prevents us to do such an extension. Thus, EoS2 has been preferred for describing the deepest layers (iron core and lower mantle). EoS1 is used for the upper mantle and for the liquid layer. Note that for the hydrosphere, we use a second order Birch–Murnaghan equation of state and the thermal expansion coefficient is constant (Table 1). The behavior of ice VII being well described with the EoS2 (Fei et al., 1993), this choice has been retained in the model.

References

Alfe, D., Price, G.D., Gillan, M.J., 2002. Iron under Earth's core conditions: Liquid-state thermodynamics and high-pressure melting curve from ab initio calculations. Phys. Rev. B 65, 118–165, doi:10.1103/PhysRevB.65.165118.

Anderson, D.L., 1980. Tectonics and composition of Venus. Geophys. Res. Lett. 7, 101–102.

Anderson, O.L., Isaak, D.L., Oda, H., 1991. Thermoelastic parameters for six minerals at high temperature. J. Geophys. Res. 96, 18037–18046.

Anderson, W.W., Ahrens, T.J., 1994. An equation of state for liquid iron and implications for the Earth's core. J. Geophys. Res. 99, 4273–4284.

Anderson, W.W., Ahrens, T.J., 1996. Shock temperature and melting in iron sulfides at core pressures. J. Geophys. Res. 101 (B3), 5627–5642.

Beaulieu, J.-P., and 71 colleagues, 2006. Discovery of a cool planet of 5.5 Earth masses through gravitational microlensing. Nature 439, 437–440.

Boehler, R., 1992. Melting of the Fe–FeO and the Fe–FeS systems at high pressure—Constraints on core temperatures. Earth Planet. Sci. Lett. 111, 217–227.

Boehler, R., 1993. Temperatures in the Earth's core from melting-point measurements of iron at high static pressures. Nature 363, 534–536.

Borde, P., Rouan, D., Léger, A., 2003. Exoplanet detection capability of the CoRoT space mission. Astron. Astrophys. 405, 1137–1144.

Bouhifd, M.A., Andrault, D., Fiquet, G., Richet, P., 1996. Thermal expansion of forsterite up to the melting point. Geophys. Res. Lett. 23, 1143–1146.

Cameron, A.G.W., Fegley, B., Benz, W., Slattery, W.L., 1988. The strange density of Mercury: Theoretical considerations. In: Vilas, F., Chapman, C.R., Matthews, M.S. (Eds.), Mercury. Univ. of Arizona Press, Tucson, AZ, pp. 692–708.

Däpen, W., 1999. Atoms and molecules. In: Cox, A.N. (Ed.), Allen's Astrophysical Quantities. fourth ed. Springer-Verlag, New York, pp. 27–51.

Dreibus, G., Wänke, H., 1985. Mars: A volatile rich planet. Meteoritics 20, 367–382.

Dubois, V., Mocquet, A., Sotin C., 2002. Effect of the chemistry of the stellar nebula on the relationship between mass and radius for Earth-like exoplanets. E.G.S. XXVII, Nice.

Duffy, T.S., Zha, C.S., Downs, R.T., Mao, H.K., Hemley, R.J., 1995. Elasticity of forsterite to 16 GPa and the composition of the upper mantle. Nature 378, 170–173.

Dziewonski, A.M., Anderson, D.L., 1981. Preliminary reference Earth model. Phys. Earth Planet. Int. 25, 297–356.

Fegley, B., Cameron, A.G.W., 1987. A vaporization model for iron/silicate fractionation in the Mercury protoplanet. Earth Planet. Sci. Lett. 82, 207–222.

Fei, Y., Mao, H., Hemley, R., 1993. Thermal expansivity, bulk modulus, and melting curve of H_2O ice VII to 20 GPa. J. Chem. Phys. 99, 5369–5373.

Frank, M.R., Fei, Y., Hu, J., 2004. Constraining the equation of state of fluid H_2O to 80 GPa using the melting curve, bulk modulus, and thermal expansivity of Ice VII. Geochim. Cosmochim. Acta 68, 2781–2790.

Hemley, R.J., Jephcoat, A.P., Mao, H.K., Zha, C.S., Finger, L.W., Cox, D.E., 1987. Static compression of H_2O-ice to 128 GPa. Nature 330, 737–740.

Hemley, R.J., Stixrude, L., Fei, Y., Mao, H.K., 1992. Constraints on lower mantle composition from P–V–T measurements of (Fe,Mg)SiO_3–perovskite and (Fe,Mg)O. In: Syono, Y., Manghnani, M.H. (Eds.), High Pressure Research: Applications to Earth and Planetary Sciences. In: AGU Monogr., vol. 67, pp. 183–189.

Hobbs, P.V., 1974. Ice Physics. Clarendon, Oxford. 837 pp.

Hubbard, W.B., Podolak, M., Stevenson, D.J., 1995. The interior of Neptune. In: Cruikshank, D.P. (Ed.), Neptune and Triton. Univ. Arizona Press, Tucson, AZ, pp. 109–138.

Huang, C., Zhao, G., Zhang, H.W., Chen, Y.Q., 2005. Chemical abundances of 22 extrasolar planet host stars. Mon. Not. R. Astron. Soc. 363, 71–78.

Irifune, T., 1987. An experimental investigation of the pyroxene—Garnet transformation in a pyrolite composition and its bearing on the constitution of the mantle. Phys. Earth Planet. Int. 45, 324–336.

Ita, J., Stixrude, L., 1992. Petrology, elasticity, and composition of the mantle transition zone. J. Geophys. Res. 97 (B5), 6849–6866.

Jackson, I., 1998. Elasticity, composition and temperature of the Earth's lower mantle: A reappraisal. Geophys. J. Int. 134, 291–311.

Javoy, M., 1995. The integral enstatite chondrite model of the Earth. Geophys. Res. Lett. 22, 2219–2222.

Javoy, M., 1999. Chemical Earth models. C. R. Acad. Sci. Paris 329, 537–555.
Kavner, A., Duffy, T.S., Shen, G., 2001. Phase stability and density of FeS at high pressures and temperatures: Implications for the interior structure of Mars. Earth Planet. Sci. Lett. 185, 25–33.
Koenig, M., and 30 colleagues, 2004. High pressures generated by laser driven shocks: Application to planetary physics. Nucl. Fusion 44, 208–214.
Kuskov, O.L., Kronrod, V.A., 2001. Core sizes and internal structure of Earth's and Jupiter's satellites. Icarus 151, 204–227.
Léger, A., Selsis, F., Sotin, C., Guillot, T., Despois, D., Mawet, D., Ollivier, M., Labèque, A., Calette, C., Brachet, F., Chazelas, B., Lammer, H., 2004. A new family of planets? "Ocean planets". Icarus 169, 499–504.
Lovis, C., and 13 colleagues, 2006. An extrasolar planetary system with three Neptune-mass planets. Nature 441, 305–309, doi:10.1038/nature04828.
Lide, D.R., 2005. Handbook of Chemistry and Physics, 85th ed. CRC Press, New York. 6.1–6.15.
Lin, D.N.C., Bodenheimer, P., Richardson, D.C., 1996. Orbital migration of the planetary companion of 51 Pegasi to its present location. Nature 380, 606–607.
Mishima, O., Endo, S., 1978. Melting curve of ice VII. J. Chem. Phys. 68, 4417–4418.
Munro, R.G., Block, S., Mauer, F.A., Piermarini, G., 1982. Isothermal equations of state for H_2O-VII and D_2O. J. Appl. Phys. 53 (9), 6174–6178.
Podolak, M., Podolak, J.I., Marley, M.S., 2000. Further investigations of random models of Uranus and Neptune. Planet. Space Sci. 48, 143–151.
Poirier, J.-P., 1994. Physical properties of the Earth's core. C. R. Acad. Sci. 318, 341–350.
Poirier, J.-P., 2000. Introduction to the Physics of the Earth Interior, second ed. Cambridge Univ. Press, Cambridge, 264 pp.
Rivera, E.J., Lissauer, J.J., Butler, R.P., Marcy, G.W., Vogt, S.S., Fischer, D.A., Brown, T.M., Laughlin, G., 2005. A ∼7.5 Earth-mass planet orbiting the nearby star GJ 876. Astron. J. 634, 625–640.
Rouan, D., Baglin, A., Barge, P., Copet, E., Deleuil, M., Léger, A., Schneider, J., Toublanc, D., Vuillemin, P., 1999. Searching for exosolar planets with the CoRoT space mission. Phys. Chem. Earth 24, 567–571.
Schwager, B., Chudinovskikh, L., Gavriliuk, A., Boehler, R., 2004. Melting curve of H_2O to 90 GPa measured in a laser-heated diamond cell. J. Phys. Condens. Matter 16, S1177–S1179.
Solomon, S.C., 1979. Formation, history and energetics of cores in the terrestrial planets. Phys. Earth Planet. Int. 19, 168–182.
Sotin, C., Tobie, G., 2004. Internal structure and dynamics of the large icy satellites. C. R. Acad. Sci. Phys. 5, 769–780.
Stevenson, D.J., 1999. Life-sustaining planets in interstellar space? Nature 400, 32.
Stixrude, L., Lithgow-Bertelloni, C., 2005. Thermodynamics of mantle minerals. I. Physical properties. Geophys. J. Int. 162, 610–632.
Stixrude, L., Wasserman, E., Cohen, R.E., 1997. Composition and temperature of Earth's inner core. J. Geophys. Res. 102, 24729–24739.
Thompson, S.L., 1990. ANEOS—Analytic Equations of State for Shock Physics Codes. Sandia Natl. Lab. Doc. SAND89-2951.
Tozer, D.C., 1972. The present thermal state of the terrestrial planets. Phys. Earth Planet. Int. 6, 182–197.
Trilling, D.E., Benz, W., Guillot, T., Lunine, J.I., Hubbard, W.B., Burrows, A., 1998. Orbital evolution and migration of giant planets. Astrophys. J. 500, 428–439.
Uchida, T., Wang, Y., Rivers, M.L., Sutton, S.R., 2001. Stability field and thermal equation of state of e-iron determined by synchrotron X-ray diffraction in a multianvil apparatus. J. Geophys. Res. 106, 21799–21810.
Vacher, P., Mocquet, A., Sotin, C., 1998. Computation of seismic profiles from mineral physics: The importance of the non-olivine components for explaining the 660 km depth discontinuity. Phys. Earth Planet. Int. 106, 275–298.
Valencia, D., O'Connel, R.J., Sasselov, D., 2006. Internal structure of massive terrestrial planets. Icarus 181, 545–554.
Volcadlo, L., de Wijs, G.A., Kresse, G., Gillan, M., Price, G.D., 1997. First principles calculations on crystalline and liquid iron at Earth's core conditions. Faraday Discuss. 106, 205–217.
Williams, Q., Jeanloz, R., Bass, J., Svendsen, B., Ahrens, T.J., 1987. The melting curve of iron to 250 gigapascals—A constraint on the temperature at Earth's center. Science 236, 181–184.
Wuchterl, G., Guillot, T., Lissauer, J.J., 2000. Giant planet formation. In: Mannings, V., Boss, A.P., Russell, S.S. (Eds.), Protostars and Planets. Univ. of Arizona Press, Tucson, p. 1081.
Yoder, C.F., Konopliv, A.S., Yuan, D.N., Standish, E.M., Folkner, W.M., 2003. Fluid core size of Mars from detection of the solar tide. Science 300, 299–303.
Yoo, C.S., Holmes, N.C., Ross, M., 1993. Shock temperatures and melting of iron at Earth core conditions. Phys. Rev. Lett. 70, 3931–3934.
Zerr, A., Diegeler, A., Boehler, R., 1998. Solidus of Earth's deep mantle. Science 281, 243–246.